Targeted Activation of OGG1 Inhibits Paraptosis in Lens Epithelial Cells of Early Age-Related Cortical Cataract

Wenjing Geng, Pengfei Li, Guowei Zhang, Renhao Zhong, Linhui Xu, Lihua Kang, Xi Liu, Miaomiao Wu, Min Ji, and Huaijin Guan

Eye Institute, Affiliated Hospital of Nantong University, Medical School of Nantong University, Nantong, Jiangsu, China

Correspondence: Min Ji, Eye Institute, Affiliated Hospital of Nantong University, Medical School of Nantong University, Nantong, Jiangsu 226001, China; amyjieye@126.com.
Huaijin Guan, Eye Institute, Affiliated Hospital of Nantong University, Medical School of Nantong University, Nantong, Jiangsu 226001, China; guanhjeye@163.com.

WG, PL, and GZ contributed equally to the study.

Received: January 28, 2024
Accepted: December 16, 2024
Published: January 13, 2025

Citation: Geng W, Li P, Zhang G, et al. Targeted activation of OGG1 inhibits paraptosis in lens epithelial cells of early age-related cortical cataract. *Invest Ophthalmol Vis Sci.* 2025;66(1):29. https://doi.org/10.1167/iovs.66.1.29

Purpose. To investigate potential modes of programmed cell death in the lens epithelial cells (LECs) of patients with early age-related cortical cataract (ARCC) and to explore early-stage intervention strategies.

Methods. Anterior lens capsules were collected from early ARCC patients for comprehensive analysis. Ultrastructural examination of LECs was performed using transmission electron microscopy. Cell death–associated protein markers were quantified via Western blot analysis, including those for paraptosis (ALIX, GRP78), apoptosis (cleaved caspase 3 and caspase 9), pyroptosis (N-GSDMD), and ferroptosis (GPX4). Intracellular vesicle–organelle colocalization was assessed through immunofluorescence. OGG1 protein expression and activity were evaluated through multiple methods, including Western blot, laser micro-irradiation, and immunofluorescence. The therapeutic potential of the OGG1 activator TH10785 on paraptosis was investigated using an ex vivo rat lens model.

Results. Morphologic changes revealed significant endoplasmic reticulum (ER) swelling in ARCC patient LECs, with no characteristic apoptotic features. Paraptosis-related proteins exhibited significant alterations, while other cell death pathway markers (apoptosis, pyroptosis, and ferroptosis) remained unchanged. In the reactive oxygen species–induced paraptosis model, vesicular structures showed exclusive colocalization with ER-specific fluorescence. Elevated levels of the DNA damage marker 7,8-dihydro-8-oxoguanine were observed concurrent with decreased OGG1 activity. The OGG1 activator TH10785 showed efficacy in suppressing LECs paraptosis in ex vivo rat lens cultures.

Conclusions. Paraptosis was identified in the LECs of patients with early ARCC. TH10785 activates OGG1 to suppress paraptosis in LECs, suggesting a novel therapeutic approach for early ARCC intervention.

Keywords: age-related cortical cataract, vacuolar degeneration, paraptosis, OGG1

Age-related cataract (ARC) is a primary cause of blindness worldwide, with a reported prevalence of 17.2%.[1] Although surgical intervention remains an effective treatment, patients in remote or impoverished areas may encounter complications that could lead to blindness.[2] Contemporary pharmacologic interventions have demonstrated limited efficacy in treating cataracts. This is mainly because lens crystallins have already denatured in late-stage cataracts, and drugs cannot effectively reverse this damage in vivo to restore transparency,[3] highlighting the urgent need for early intervention strategies. Therefore, we aimed to intervene in the early pathologic stages of age-related cortical cataract (ARCC). The earliest sign of ARCC under slit-lamp microscopy is vacuole formation in the anterior or equatorial cortical regions of the lens.[4] With the progression of ARCC, lens opacity begins to appear. It has been reported that if the cataratogenic stimulus is withdrawn, the watery vacuoles in the lens cortex may be reversible.[5] This provides a theoretical foundation for our intervention during the early pathologic stages of ARCC. The homeostasis of fiber cells and the clarity of the lens depend on the function of its overlying epithelium.[6] To date, no studies have explored the pathologic changes in lens epithelial cells (LECs) during the early stages of ARCC.

ARC is influenced by multiple risk factors, including aging, ultraviolet B radiation exposure, and lifestyle factors such as smoking and alcohol consumption.[7] These diverse pathogenic factors converge on a common molecular mechanism: the induction of oxidative stress in LECs.[8] LECs form a vital monolayer covering the anterior lens surface, serving as the primary regulatory interface for lens homeostasis.[9] Consequently, LECs may already be affected by oxidative stress before vacuole in early ARCC. While apoptosis represents the predominant mode of cell death in LECs,[10] emerging research has revealed significant contributions of ferroptosis[11] and autophagy[12] in the pathogenesis of ARC. However, the participants in these studies were patients with moderate or advanced ARC exhibiting cuneiform opacity, and the precise pathologic mechanisms underlying early ARCC remain poorly understood.[13] Paraptosis, a distinct form of programmed cell death, has been increasingly recognized as a significant contributor to the early pathologic

processes in age-related diseases.[14] It is characterized by extensive abnormal dilation of the endoplasmic reticulum (ER) and/or mitochondria, without nuclear fragmentation, chromatin condensation, or formation of apoptotic bodies.[15] Of particular interest, some studies have observed the vacuolating cytoplasmic changes in LECs of presenile cataract patients.[16,17] Nevertheless, the potential role of paraptosis as a mechanism of LECs death during the early stages of ARCC requires further investigation.

Reactive oxygen species (ROS), recognized as principal mediators of paraptosis, play a pivotal role in the pathogenesis of ARC. They induce extensive oxidative damage to DNA bases,[18] with 7,8-dihydro-8-oxoguanine (8-oxoG) serving as a well-established marker of DNA oxidative damage. Notably, significantly elevated levels of 8-oxoG have been documented in LECs from ARC patients.[19] In the cellular defense against such oxidative insults, 8-oxoguanine deoxyribonucleic acid glycosylase 1 (OGG1) emerges as a crucial enzyme within the base excision repair pathway, specifically recognizing and eliminating 8-oxoG lesions. Our previous research has demonstrated that diminished OGG1 activity significantly contributes to ARC progression.[19] However, the precise mechanistic role of OGG1 during the early pathologic stages of ARCC remains to be fully delineated.

In this study, we employed transmission electron microscopy (TEM) to characterize the ultrastructural features of LECs in early ARCC. Mechanistically, we evaluated the expression profiles of protein markers associated with various forms of programmed cell death, including paraptosis, apoptosis, pyroptosis, and ferroptosis. Our findings revealed that ROS-induced paraptosis may represent a predominant mode of programmed cell death in LECs during early ARCC development. To explore potential therapeutic interventions for early ARCC, we investigated the efficacy of the OGG1 activator TH10785 in modulating paraptosis, both in LECs exposed to low-concentration H_2O_2 and in an ex vivo rat lens model. Collectively, our study elucidates the distinctive pathologic characteristics of early-stage ARCC, suggesting that targeted intervention during this critical period may provide a promising novel therapeutic strategy for ARCC management.

Materials and Methods

Human Samples

This study was approved by the Ethics Committee of the Affiliated Hospital of Nantong University. All patients signed informed consent according to the tenets of the Declaration of Helsinki. The anterior lens capsules of transparent lenses were sourced from cadaveric eyes at the eye bank of the Nantong Red Cross. Additionally, the anterior lens capsules were collected from patients with early ARCC aged over 50 years who exhibited localized or beaded vacuoles in the lens cortex under slit-lamp microscopy, affecting visual function. The exclusion criteria included high myopia, uveitis, eye trauma, glaucoma, previous intraocular surgeries in either eye, and systemic diseases, such as diabetes mellitus and autoimmune disease. The anterior lens capsules were obtained by the same experienced surgeon during capsulorrhexis. The tissue samples were immediately frozen in liquid nitrogen and stored at −80°C for Western blotting. A self-made 20-gauge syringe needle was then used to extract the vacuolar cortex. The cortex was fixed in 4% paraformaldehyde and stained with hematoxylin and eosin (H&E). The remaining cortex was fixed with 2.5% glutaraldehyde and observed using TEM.

Experimental Animals

Sprague-Dawley (SD) rats were obtained from the Laboratory Animal Center of Nantong University. Their care was in accordance with the guidelines established by ARVO regarding animal use in research. The Institutional Ethics Committee for Animal Experimentation at Nantong University approved all experimental procedures involving these animals and ensured adherence to established institutional guidelines (No. S20210226-051).

Cell Culture and Treatment

The LEC line (SRA01/04) was supplied by Professor Yao Ke from Zhejiang University, and authentication was performed by Suzhou Genetic Testing Biotech Co., Ltd. (Suzhou, China) via STR profiling to verify their identity.[20] This cell line was maintained in Dulbecco's modified Eagle's medium (Gibco Rockville, MD, USA), enriched with 10% fetal bovine serum (Gibco) and supplemented with 100 IU/mL penicillin-streptomycin (Procell, Wuhan, China). The culture conditions were maintained at 37°C in an atmosphere containing 5% CO_2. LECs were treated with hydrogen peroxide (H_2O_2) at varying concentrations (0, 25, 50, 100, 200, and 400 µM) for 24 hours. Withaferin-A (WA) (MCE, Monmouth Junction, NJ, USA), an inducer of paraptosis, was used at 3 µM for 12 hours. ZVAD-FMK (Beyotime Biotechnology, Shanghai, China), a pan-caspase inhibitor, was pretreated at 10 µM for 2 hours. TH10785 (MCE), an OGG1 activator, was used at 10 µM for 8 hours. TH5487 (MCE), an OGG1 inhibitor, was used at 10 µM for 8 hours.

Hematoxylin and Eosin Staining

The vacuolar cortex was fixed with 4% paraformaldehyde, embedded in paraffin, and sectioned to a thickness of 5 to 6 µm. These sections were prepared in paraffin and stained with H&E. Subsequently, the sections were dewaxed and hydrated using a series of xylene and alcohol treatments. Images were recorded using an inverted microscope (DMi8; Leica, Wetzlar, Germany).

Immunofluorescence Staining

LECs were fixed with 4% paraformaldehyde for 30 minutes at room temperature. Blocking and permeabilization were performed in a solution containing 0.1% Triton X-100 and 3% bovine serum albumin for an hour at room temperature. The cells were incubated with anti–oxoguanine-8 antibody (1:50, ab206461; Abcam, Cambridge, MA, USA) diluted in the blocking buffer overnight at 4°C. After washing with PBS for three times, the cells were incubated with the corresponding secondary antibody, Alexa Fluor 568 goat anti-mouse IgG (1:250, 31160; Invitrogen, Carlsbad, CA, USA), for 2 hours at room temperature in the dark. DAPI was used to visualize cell nuclei. Images were captured using a fluorescence microscope (LSM 900; Carl Zeiss Meditec, Jena, Germany).

Investigative Ophthalmology & Visual Science

Measurement of Reactive Oxygen Species

ROS generation was measured using a CM-H2DCFDA probe (Invitrogen) according to the manufacturer's instructions. Briefly, LECs were plated into 24-well plates at a density of 8×10^4 cells per well. The cells underwent incubation with a 10-µM solution of CM-H2DCFDA dye for 30 minutes at 37°C. The plates were then washed with PBS. Images were captured using a fluorescence microscope (DMi8; Leica).

For human lens epithelium, a mixed staining solution containing 10 µM CM-H2DCFDA and Hoechst (1:1000) was prepared in advance. After obtaining fresh lens epithelium, the sample was immediately immersed in the staining solution and incubated at 37°C for 30 minutes, followed by two washes with PBS. The lens epithelium was then spread onto a glass slide, and images were promptly captured using a fluorescence microscope (LSM 900; Carl Zeiss Meditec).

Transmission Electron Microscopy

The lens capsules and cortex and LECs were fixed in 2.5% glutaraldehyde in phosphate buffer. Subsequently, the specimens were washed with phosphate buffer and fixed in % OsO_4 in phosphate buffer for 1 hour. After dehydration in graded ethanol solutions, the specimens were embedded in epoxy resin. Ultrathin sections were observed using a TEM (HITACHI, Tokyo, Japan).

Live-Cell Imaging

ER-Tracker green (Beyotime Biotechnology), Mito-Tracker red (Beyotime Biotechnology), Lyso-Tracker red (Beyotime Biotechnology), DAPRed (DOJINDO, Kumamoto, Japan), ECGreen (DOJINDO), and Lucifer yellow (Invitrogen) were used to label the ER, mitochondria, lysosomes, autophagosomes, endosomes, and macropinosomes, respectively, according to the manufacturers' instructions. LECs were plated on 35-mm glass bottom dishes (Cellvis, Mountain View, CA, USA) and treated with 50 µM H_2O_2 for 24 hours. Subsequently, the cells were incubated with medium containing ER-Tracker Green, Mito-Tracker Red, Lyso-Tracker Red, DAPRed, and ECGreen for 30 minutes, while Lucifer Yellow was incubated for 10 minutes. The cells were then washed with PBS, and images were captured using fluorescence microscopes (HIS-SIM [Guangzhou, China] and LSM 900 [Carl Zeiss Meditec]).

Cell Viability Assay

An Enhanced Cell Counting Kit-8 (CCK-8) (DOJINDO) was used to measure cell viability. LECs were plated into 96-well plates at a density of 1×10^4 cells per well. After different treatments of LECs, 10 µL CCK-8 reagent was added to each well. The plates were evaluated using a microplate reader (Invitrogen) after 2 hours of incubation at 37°C with 5% CO_2.

Reverse Transcription–Quantitative Real-Time PCR

Three anterior lens capsules from the same group were pooled as one sample, and each group contained three pooled samples. The samples were stored at –80°C before RNA purification. Total RNA from rat lens capsules was extracted using TRIzol reagent (Invitrogen). Total RNA was quantified using a Nanodrop 2000 (Thermo Scientific, Wilmington, DE, USA) and then reverse-transcribed into cDNA using the HiScript III RT Supermix Kit (Vazyme, Nanjing, China). A combination of Oligo (dT) and random hexamer primers was used for cDNA synthesis, with 600 ng RNA used per reverse transcription reaction. Quantitative real-time PCR was performed with the ChamQ Universal SYBR qPCR Master Mix Kit (Vazyme). Primers were designed to span introns, and no-reverse-transcriptase reactions were included as controls. Technical replicates were conducted three times, with an acceptable variation in Cq values of no more than 0.2. The relative expression levels of mRNAs were calculated using the $2^{-\Delta\Delta Ct}$ method and normalized to *GAPDH*. Primer details for the amplification process are provided in Supplementary Table S1.

Western Blotting

RIPA buffer supplemented with protease and phosphatase inhibitors (Beyotime Biotechnology) was utilized to lyse lens capsules or LECs. The total protein concentration was determined using a BCA Protein Assay Kit (Invitrogen). Subsequently, the protein samples were separated on SDS-polyacrylamide gels and transferred to 0.22-µm polyvinylidene fluoride membranes (Millipore, Burlington, MA, USA). The membrane was blocked with 5% nonfat milk in TBST for 2 hours at room temperature and incubated overnight at 4°C with primary antibodies (listed in Supplementary Table S2). The membranes were washed with TBST three times and incubated with diluted goat anti-rabbit or mouse IgG-HRP (Santa Cruz Biotechnology, Dallas, TX, USA) for 2 hours at room temperature. The protein bands were scanned using an enhanced chemiluminescence method (Vazyme) and quantified using the ImageJ software (National Institutes of Health, Bethesda, MD, USA).

Laser Micro-Irradiation

LECs were transfected with the OGG1-mCherry (Public Plasmid Library, Nanjing, China) vector and selected with 1 µg/mL puromycin (Beyotime Biotechnology). LECs stably expressing mCherry-tagged wild-type OGG1 were plated on a 35-mm glass bottom plate for 24 hours. For laser microirradiation, LECs were presensitized with 5 µg/mL Hoechst 33342 (Beyotime Biotechnology) for 10 minutes at 37°C. Subsequently, the LECs were transferred to a 37°C chamber attached to a confocal microscope (LSM 900; Carl Zeiss Meditec). DNA damage was induced by selecting a nuclear spot (10×10 pixels) using the ZEN software's circular region tool (ZEN; Carl Zeiss Meditec) and exposing it to a 405-nm diode laser at 100% power (spot irradiation, one iteration, zoom 4, and pixel dwell time of 14.29 µs). Quantitative analysis involved evaluating recruitment kinetics by adjusting the fluorescence intensity at the irradiated spot and assessing the total nuclear fluorescence loss over time. Normalization was performed at the preirradiation level. The experiments were performed in duplicate, and six cells were assessed per experiment.

Lens Organ Culture Ex Vivo

Adult SD rats were sacrificed by intraperitoneal injection of excess pentobarbital sodium. The intact rat lenses were separated without destroying the lens capsule in PBS buffer. The lenses were transferred into 1 mL serum-free M199 medium (Gibco) with an antibiotic mixture at 37°C with 5% CO_2.

Investigative Ophthalmology & Visual Science

Approximately 24 hours after lens preparation, transparent lenses were selected and cultured within M199 medium in the control group or 50 μM H_2O_2 and 50 μM H_2O_2 + 10 μM TH10785 treatments in the experimental groups.

Statistical Analysis

All experiments were repeated at least three times, and the data are presented as the mean ± SEM. Statistical analyses were performed using the GraphPad Prism 8.0 software (GraphPad Software, La Jolla, CA, USA). The analysis involved a Student's *t*-test for two-group comparisons and a one-way ANOVA for more than two groups. Statistical significance was established at a P value < 0.05.

Results

Paraptosis Occurs in the LECs of Early ARCC

We frequently observed isolated or beaded vacuoles in the superficial cortex of early ARCC patients under a surgical microscope (Fig. 1A). H&E staining revealed disordered fiber arrangement and enlarged intercellular spaces in the vacuolar cortex, while no Morgagnian globules were observed (Fig. 1B). The arrangement and morphology of the cortical fibers observed by TEM were consistent with those seen in H&E staining (Fig. 1C). The ultrastructure of LECs was examined using TEM, revealing notable ER dilation, with intact cell membranes, nuclear envelopes, and normal chromatin distribution (Fig. 1D). These ultrastructural features are inconsistent with the typical morphologic characteristics of apoptosis and more closely align with those observed in paraptosis. Although various forms of programmed cell death are difficult to decipher conclusively and exclusively, specific markers may assist in identification. To determine whether early ARCC is associated with paraptosis, we examined markers of paraptosis and several other cell death modalities reported in cataracts, including apoptosis, pyroptosis, and ferroptosis, within the lens epithelium of patients with early ARCC. In comparison with transparent human lenses, the expression levels of paraptosis-related proteins GRP78, p-ERK, and p-P38 were increased, whereas ALIX was decreased in the LECs of early ARCC patients (Figs. 1E, 1F). Compared to the positive controls, the cleaved forms of caspase 3 and caspase 9 were not detected in either group (Fig. 1G). Additionally, the pyroptosis execution protein N-GSDMD was not identified (Fig. 1H). There was no significant difference in the levels of the ferroptosis marker protein GPX4 between the two groups (Figs. 1I, 1J). We also examined autophagy components, including P62, BECN1, and LC3B. In the early ARCC group, the levels of P62 and BECN1 were significantly elevated, whereas LC3B showed no significant difference (Figs. 1I, 1J). In summary, these data suggest that paraptosis may be the predominant mode of cell death in LECs during the early stages of ARCC.

ROS Induces Paraptosis in LECs

ROS is a key mechanism that induces paraptosis. ROS generation was increased in the lens epithelium of patients with early ARCC (Supplementary Fig. S1). To explore whether ROS serves as a potential mechanism for paraptosis in LECs of early ARCC, we treated LECs with different concentrations of H_2O_2. After a 24-hour exposure of LECs to H_2O_2 from 25 to 400 μM, compared to the control group, ALIX expression decreased with the 50-μM H_2O_2 treatment, while GRP78 expression increased. The BAX/BCL-2 expression ratio showed no significant difference (Figs. 2A, 2B). However, at a concentration of 200 μM H_2O_2, the BAX/BCL-2 ratio significantly increased (Figs. 2A, 2B). TEM observations revealed extensive vacuolization of the ER in cells exposed to 50 μM H_2O_2 compared to control cells (Fig. 2C). To further investigate the origin of vesicles induced by 50 μM H_2O_2, we conducted live-cell staining with fluorescent trackers targeting the ER, mitochondria, lysosomes, autophagosomes, endosomes, and macropinosomes. Interestingly, the vesicles exclusively colocalized with ER fluorescence, without colocalization with any other trackers (Figs. 2D, 2E). Additionally, treatment with 50 μM H_2O_2 significantly increased the paraptosis-related protein levels of GRP78, p-ERK, and p-P38, whereas ALIX expression inversely decreased (Figs. 2F, 2G). The morphology and protein expression in cells treated with 50 μM H_2O_2 were consistent with those observed in cells treated with the paraptosis inducer, WA (Supplementary Fig. S2). To determine whether apoptosis was involved in the cell death of LECs mediated by 50 μM H_2O_2, we pretreated the LECs with ZVAD-FMK, a pan-caspase inhibitor. ZVAD-FMK failed to reduce cell death induced by 50 μM H_2O_2; however, it significantly decreased cell death caused by 200 μM H_2O_2, although not eliminating it (Fig. 2H). Taken together, these data indicate that ROS induces paraptosis in LECs.

Activation of OGG1 Inhibits ROS-Induced LEC Paraptosis

The immunofluorescence results showed significant accumulation of 8-oxoG in the LECs treated with 50 μM H_2O_2 (Figs. 3A, 3B), and OGG1 expression significantly increased (Figs. 3C, 3D). To assess the regulatory role of OGG1 in paraptosis in LECs, we enhanced its expression through liposome-mediated transient transfection. However, OGG1 overexpression did not positively regulate the expression of paraptosis-related proteins (Supplementary Fig. S3). These results indicate that simply increasing OGG1 expression levels could not inhibit paraptosis. OGG1 specifically recognizes and excises 8-oxoG generated in double-stranded DNA through its DNA glycosylase and β,δ-lyase activities.[21] The laser micro-irradiation experiment demonstrated that in LECs treated with 50 μM H_2O_2, OGG1-mCherry recruitment kinetics was impaired, as exemplified by a reduced accumulation of OGG1-mCherry. However, the addition of the OGG1 activator TH10785 significantly increased OGG1's recruitment to sites of DNA damage (Figs. 3E, 3F). Subsequently, we evaluated the effects of TH10785 on ROS-induced paraptosis in LECs. It was found that TH10785 significantly inhibited the protein levels of GRP78, p-ERK, and p-P38 under H_2O_2 treatment, while increasing the level of ALIX (Figs. 3G, 3H). Morphologically, TH10785 significantly alleviated the dilated ER (Figs. 3I, 3K). TH10785 also effectively reduced the elevated cellular ROS levels in LECs induced by treatment with 50 μM H_2O_2 (Figs. 3J, 3L). To strengthen our findings regarding OGG1's role in paraptosis, we employed the OGG1-specific inhibitor TH5487.[22] Compared to the H_2O_2 group, cotreatment with TH5487 and H_2O_2 further increased the expression levels of GRP78, p-ERK, and p-P38 while inhibiting the expression of ALIX (Supplementary Fig. S4). In brief, the inhibition of OGG1 activity exacerbated paraptosis.

It has been reported that the kinase activity of insulin-like growth factor I receptor (IGFIR) may be involved in para-

Investigative Ophthalmology & Visual Science

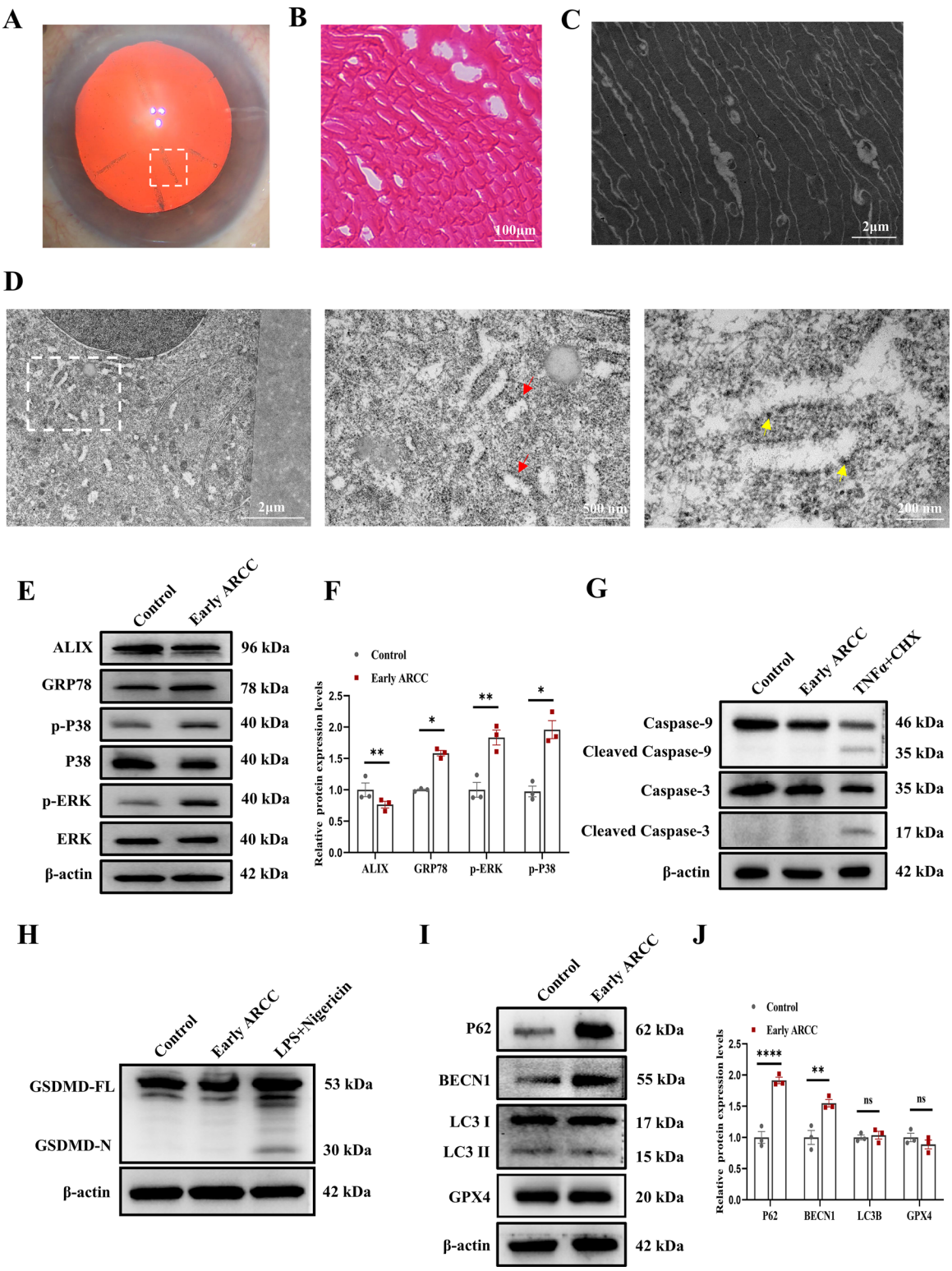

Figure 1. Paraptosis occurs in the LECs of early ARCC. (**A**) Representative surgical microscope images of lens vacuolar degeneration cortex from patients with early ARCC. The *white dotted box* indicates the cortical vacuolar degenerative area. (**B**, **C**) Representative H&E staining and TEM images of lens vacuolar degeneration cortex from patients with early ARCC. (**D**) Representative TEM images of LECs from patients with early ARCC. The *red arrows* indicate the dilated ER, and the *yellow arrows* highlight the ribosomes attached to the rough ER. (**E**, **F**) Representative Western blot bands and statistical analysis of ALIX, GRP78, p-ERK, and p-P38 expression levels in the lens epithelium of transparent human lenses (control group) and patients with early ARCC (early ARCC group). (**G**) The expression levels of apoptosis-associated proteins (cleaved forms of caspase 9 and caspase 3) in the two groups. The HeLa cells treated 7 hours with 30 ng/mL TNF-α and 10 μg/mL cycloheximide (CHX) apoptosis system served as a positive control. (**H**) The expression levels of the pyroptosis-associated protein (N-GSDMD) in the two groups. The RAW 264.7 cells pretreated 4 hours with 1 μg/mL lipopolysaccharide, then stimulated with nigericin for 12 hours, served as a positive control. (**I**, **J**) Representative Western blot bands and statistical analysis of P62, BECN1, LC3B, and GPX4 expression levels in the two groups. Data are displayed as mean ± SEM from three independent experiments. *$P < 0.05$, **$P < 0.01$, ****$P < 0.0001$, ns = no statistical significance.

Investigative Ophthalmology & Visual Science

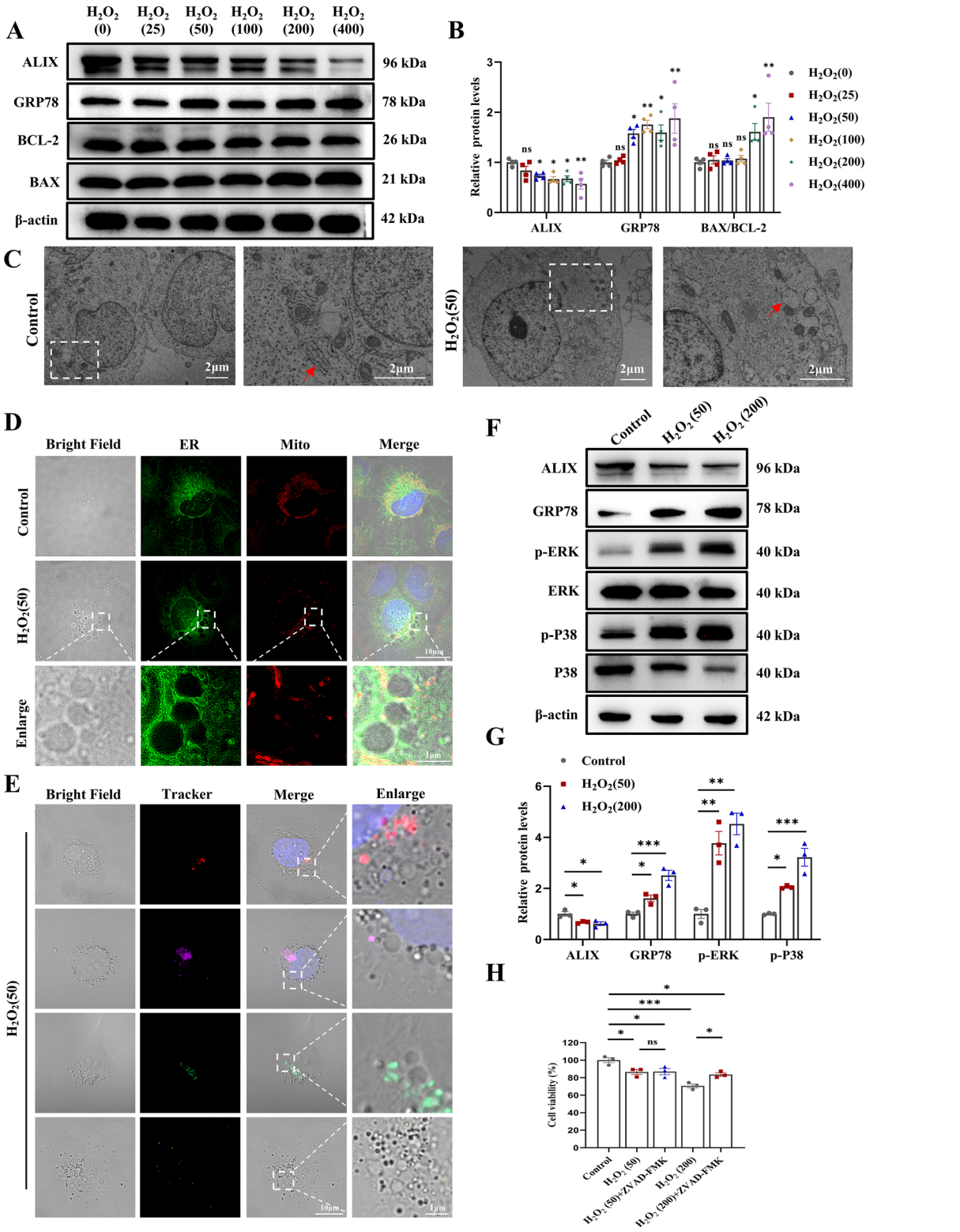

Figure 2. ROS induces paraptosis in LECs. (**A**, **B**) LECs were treated with different concentrations of H_2O_2 (0 µM, 25 µM, 50 µM, 100 µM, 200 µM, and 400 µM) for 24 hours; the Western blot images and statistical analysis displayed the relative protein expression levels of ALIX, GRP78, and the BAX/BCL-2 ratio, normalized to β-actin. (**C**) The ultrastructure of LECs was observed by TEM after a 24-hour treatment with 50 µM H_2O_2. The *red arrows* indicate the ER. (**D**) After LECs were exposed to 50 µM H_2O_2 for 24 hours, ER and mitochondria were labeled with ER-Tracker green and Mito-Tracker red, respectively. (**E**) After LECs were exposed to 50 µM H_2O_2 for 24 hours, lysosomes were labeled with Lyso-Tracker red (*red*), autophagosomes with DAPRed (*violet*), endosomes with ECGreen (*lime green*), and macropinosomes with Lucifer yellow (*yellow*). (**F**, **G**) The Western blot images and statistical analysis display the relative protein expression levels of ALIX, GRP78, p-ERK, and p-P38, normalized to β-actin, after treatment with 50 µM and 200 µM H_2O_2 for 24 hours. (**H**) Cell viability of LECs was assessed following treatment with 50 µM or 200 µM H_2O_2 for 24 hours, in the presence or absence of 10 µM ZVAD-FMK pretreated for 2 hours. Data are displayed as mean ± SEM from three independent experiments. $^*P < 0.05$, $^{**}P < 0.01$, $^{***}P < 0.001$, ns = no statistical significance.

Investigative Ophthalmology & Visual Science

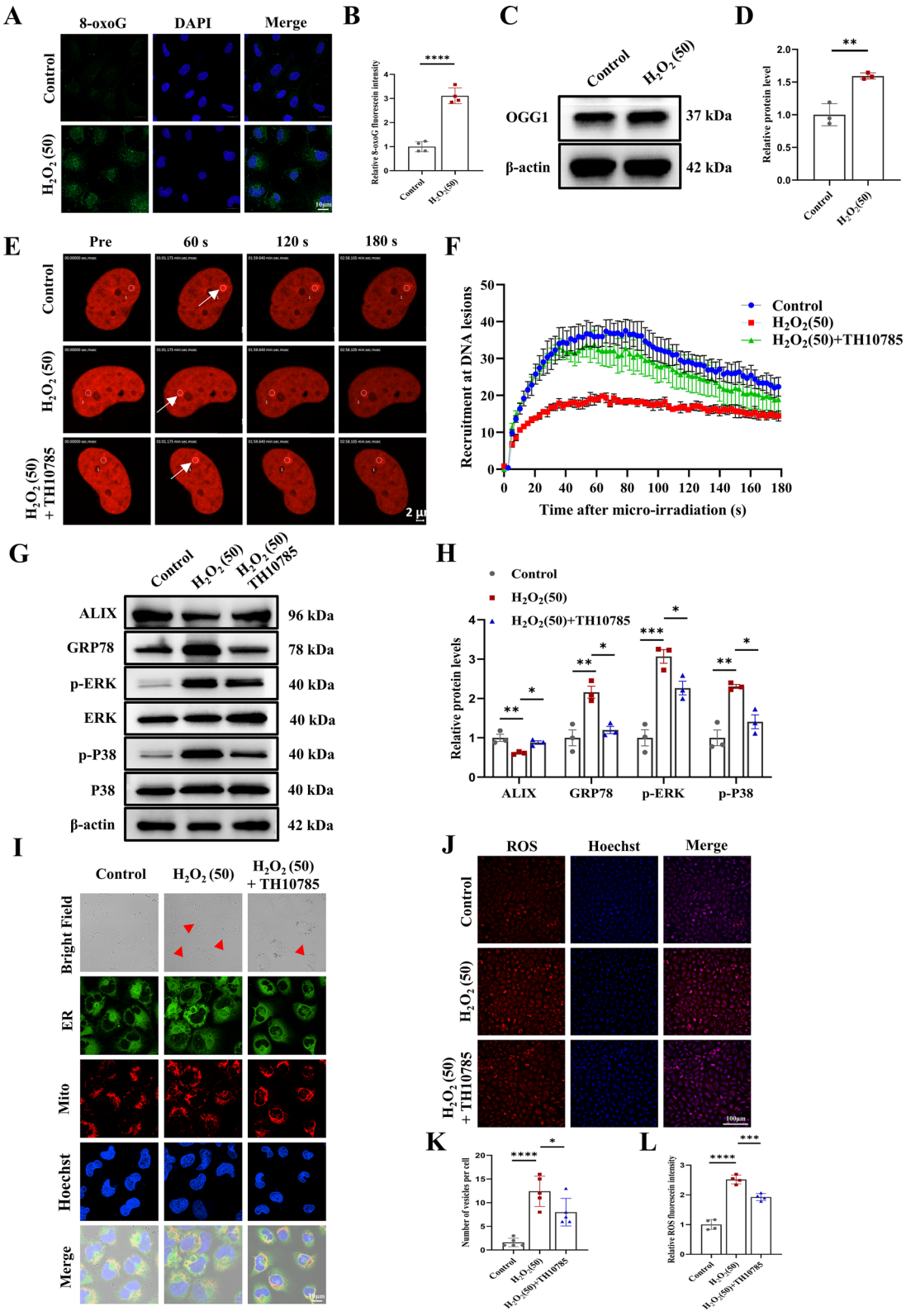

Figure 3. Activation of OGG1 inhibits ROS-induced LEC paraptosis. (**A**) Representative immunofluorescence images of indicated LECs against 8-oxoG. (**B**) Quantification and statistical analysis of 8-oxoG fluorescence intensity. (**C**, **D**) The Western blot images and statistical analysis display the relative protein expression levels of OGG1, normalized to β-actin, after treatment with 50 μM H_2O_2 for 24 hours. (**E**) Representative confocal images of OGG1-mCherry LECs following treatment at the indicated time points after laser micro-irradiation sites pointed by *white arrows*. (**F**) Connecting lines of mean values representing OGG1-mCherry recruitment kinetics. (**G**, **H**) The Western blot images and statistical analysis display the relative protein expression levels of ALIX, GRP78, p-ERK, and p-P38, normalized to β-actin. (**I**) ER and mitochondria were labeled with ER-Tracker green and Mito-Tracker red, respectively, after LECs were treated as indicated. *Red arrowheads* indicate the dilated ER. (**K**) Quantification and statistical analysis of intracellular vesicles. (**J**, **L**) Representative images of ROS generation and statistical results of indicated LECs treated with 50 μM H_2O_2 and 10 μM TH10785. Data are displayed as mean ± SEM from three independent experiments. *$P < 0.05$, **$P < 0.01$, ***$P < 0.001$, ****$P < 0.0001$.

Investigative Ophthalmology & Visual Science

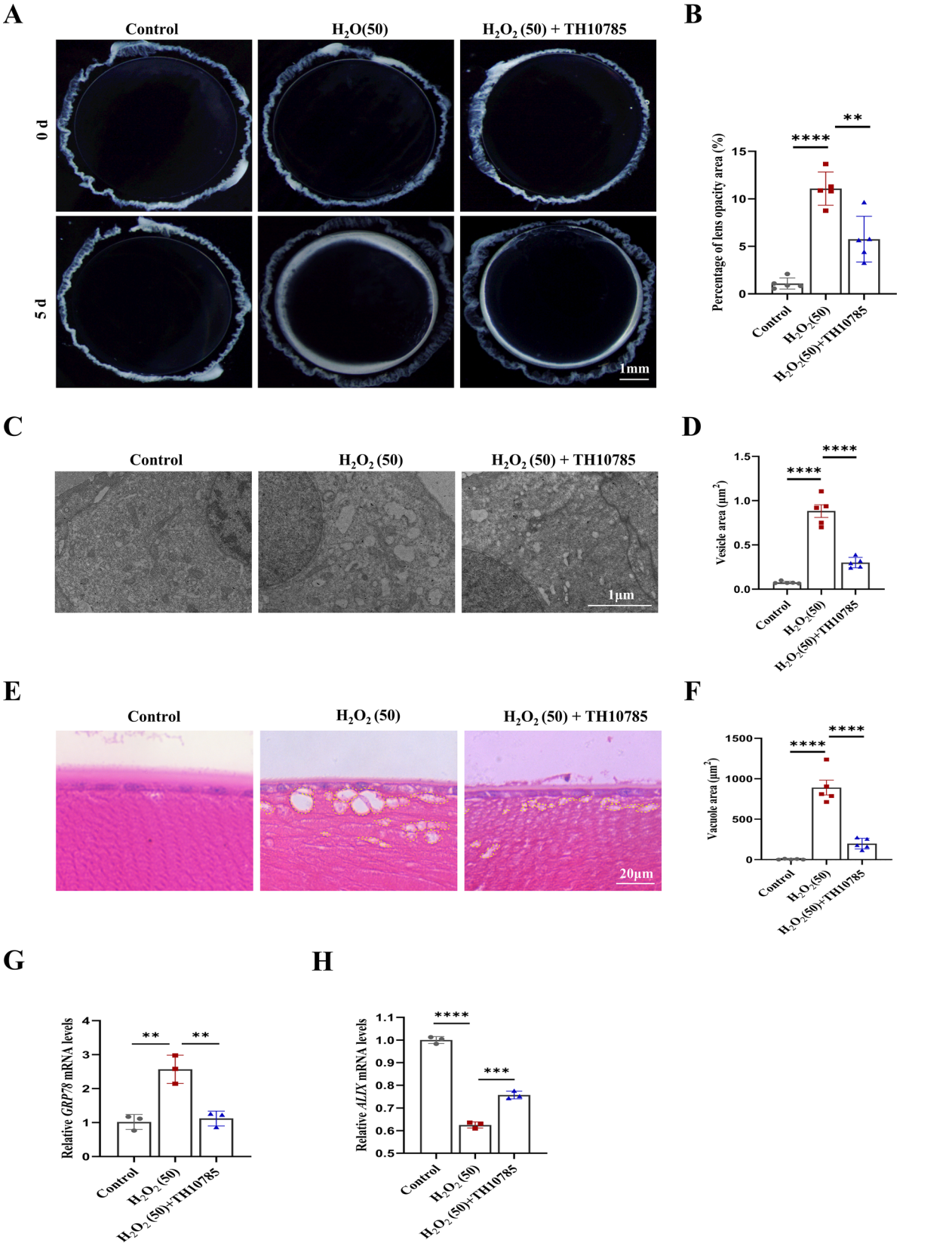

Figure 4. Effects of TH10785 on ROS-induced paraptosis and vacuoles in rat lens. Rat lenses were subjected to control, H_2O_2 (50 μM), and H_2O_2 (50 μM) with TH10785 (10 μM) medium for 5 days. (**A**, **B**) Representative images of cultured rat lenses and the percentage of lens opacity in the control, H_2O_2, and H_2O_2 + TH10785 groups. (**C**, **D**) TEM showed that TH10785 treatment alleviated the dilated ER in LECs under H_2O_2 stress. (**E**, **F**) H&E staining shows that TH10785 treatment reduced the area of vacuoles in the superficial cortex of rat lenses. (**G**, **H**) Reverse transcription–quantitative real-time PCR was performed to detect the mRNA levels of paraptosis-related genes (*GRP78* and *ALIX*) in the LECs. Data are displayed as mean ± SEM from three independent experiments. $^{**}P < 0.01$, $^{***}P < 0.001$, $^{****}P < 0.0001$.

Investigative Ophthalmology & Visual Science

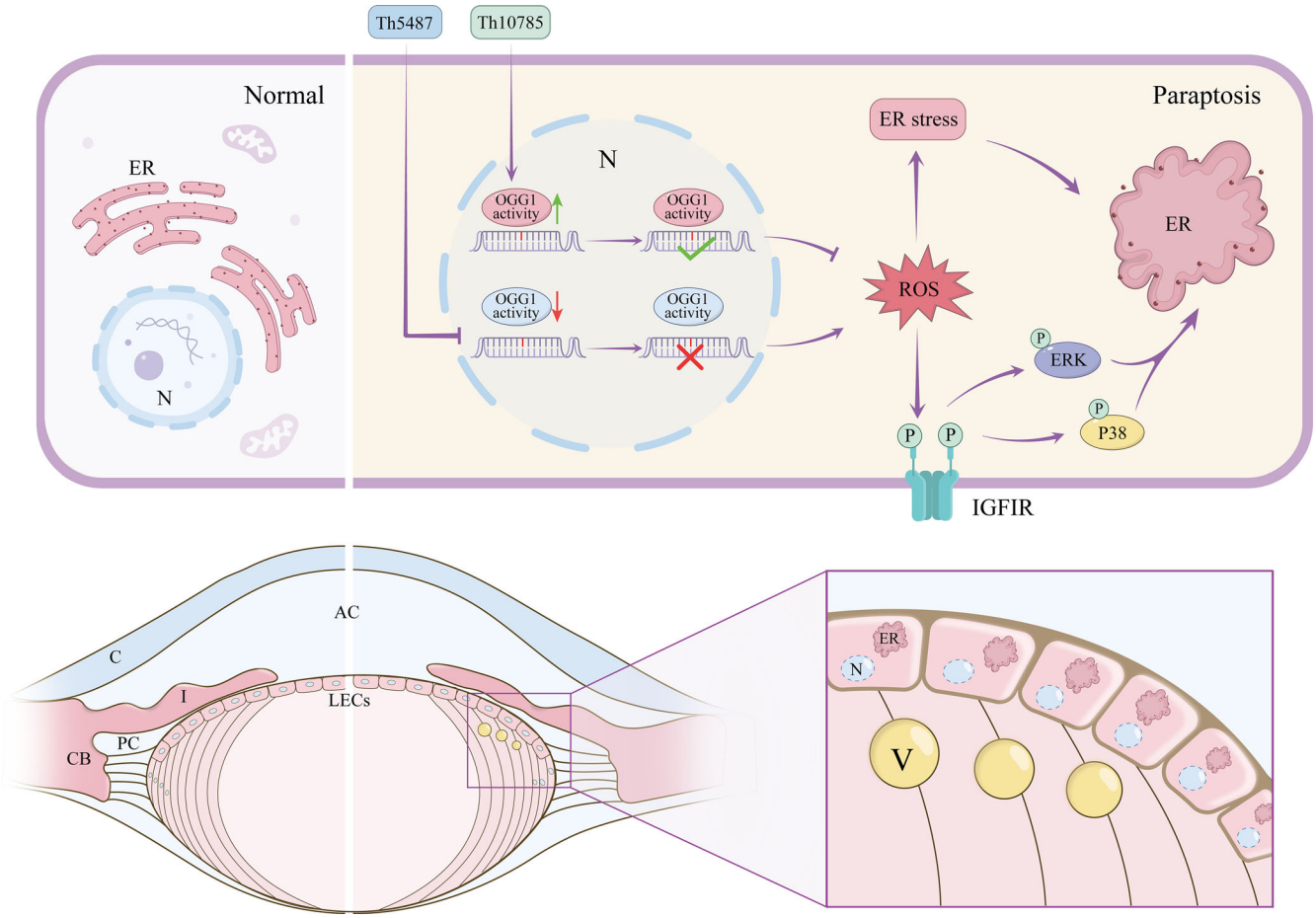

Figure 5. Schematic illustrating the mechanism of ROS-induced paraptosis in LECs of early ARCC patients. This comprehensive mechanism reveals that the elevated ROS orchestrates a cascade of cellular events, including ER stress induction, IGFIR activation, and subsequent mitogen-activated protein kinase pathway signaling. These molecular events result in ER dilation-formed intracellular vesicles and, ultimately, paraptosis in LECs. Notably, TH10785-mediated enhancement of OGG1 activity effectively suppresses ROS-induced paraptosis and vacuolar degeneration in the superficial lens cortex. AC, anterior chamber; C, cornea; CB, ciliary body; I, iris; N, nucleus; PC, posterior chamber; V, vacuoles.

ptosis.[23] Clinical specimens analysis revealed significantly elevated IGFIR phosphorylation in LECs of early ARCC patients compared to transparent human lenses (Supplementary Figs. S5A, S5B). Enhanced IGFIR phosphorylation was also observed in the in vitro paraptosis model (Supplementary Figs. S5C, S5D). Consistent with previous findings in C2C12 myocytes showing H_2O_2-induced IGFIR phosphorylation and its attenuation by ROS inhibition,[24] our results revealed significant reduction in IGFIR phosphorylation following TH10785 treatment in LECs (Supplementary Figs. S5E, S5F). These findings suggested that ROS-mediated activation of IGFIR might be involved in paraptosis. The demonstrated ability of TH10785 to attenuate IGFIR phosphorylation further supports its potential as an optimal therapeutic candidate for inhibiting ROS-induced paraptosis in LECs.

Effects of TH10785 on ROS-Induced Paraptosis and Vacuoles in Rat Lens

The results above indicate that OGG1 plays an inhibitory role in the paraptosis of LECs; therefore, we conducted ex vivo rat lens culture experiments to determine whether paraptosis occurs in rat lenses when treated with low concentrations of H_2O_2 and whether an OGG1 activator could suppress this process. The lenses in the 50-µM H_2O_2 group exhibited obvious opacities in the peripheral cortex on day 5. Interestingly, when TH10785 was added to the H_2O_2-stressed lenses, only mild opacities were observed in the peripheral cortex (Figs. 4A, 4B). In the lenses of the 50-µM H_2O_2 group, there was dilation of the ER in LECs and prominent vacuoles in the superficial cortex; moreover, TH10785 largely reversed these changes (Figs. 4C–F). Meanwhile, reverse transcription–quantitative real-time PCR analysis revealed an increase in *GRP78* mRNA levels and a decrease in *ALIX* mRNA levels in H_2O_2-stressed rat LECs, which were reversed by treatment with TH10785 (Figs. 4G, 4H).

Discussion

The reversal of cataract formation remains a formidable challenge in ophthalmology. Despite the identification of several compounds capable of reversing crystallin aggregation, none have successfully transitioned to clinical application. This limitation has prompted our investigation into

the fundamental pathogenic mechanisms underlying early ARC formation, with the goal of developing targeted therapeutic interventions. First, we identified paraptosis as a novel mode of programmed cell death in LECs during early ARCC. We subsequently conducted a comprehensive assessment of various cell death mechanisms previously documented in cataract literature, including apoptosis, pyroptosis, and ferroptosis, to evaluate their presence and relative contributions in LECs of early ARCC. Mechanistically, oxidative damage repair protein OGG1 may serve as a promising therapeutic target for paraptosis intervention. To validate this hypothesis, we employed an ex vivo rat lens culture model and demonstrated that the OGG1 activator TH10785 effectively suppressed paraptosis in LECs. This intervention successfully mitigated early pathologic alterations in the lens and impeded ARCC progression. Our research suggests that early therapeutic intervention through mechanism-based drug therapy may represent a viable strategy for preventing or delaying ARCC progression.

Paraptosis represents a unique and distinct modality of programmed cell death that exhibits fundamental differences from classical apoptosis.[25] Morphologically, paraptosis is characterized by extensive cytoplasmic vacuolization involving the dilation of the ER and/or mitochondria. Notably, this process occurs in the absence of typical apoptotic features, such as nuclear fragmentation, chromatin condensation, and apoptotic bodies formation.[15] In our study, we observed significant dilation of the ER in LECs from patients with early ARCC. Mechanistically, ROS serve as the primary initiating factor of paraptosis.[26] The kinase activity of IGFIR, along with the activation of the mitogen-activated protein kinase signaling pathway, is also associated with paraptosis, which is specifically inhibited by ALIX.[23] ER stress also contributes to the development and progression of paraptosis due to extensive ER dilation. Herein, we observed significant alterations in the expression profiles of paraptosis-related proteins within the lens epithelium of early ARCC specimens. To validate these clinical observations, we established in vitro cell models utilizing both specific paraptosis inducers and low-concentration H_2O_2 treatments, which successfully recapitulated the paraptotic phenomena observed in patient samples.

While apoptosis is well established as the predominant mode of cell death in LECs during mature ARCC,[27,28] recent studies have suggested potential roles for pyroptosis and ferroptosis in ARC development.[11,29] However, the involvement of these cell death mechanisms in early ARCC remains largely unexplored. Morphologically, TEM revealed no distinctive morphologic features characteristic of apoptosis, pyroptosis, or ferroptosis in early ARCC specimens. Mechanistically, neither cleaved caspase 3 nor caspase 9 was detected in the lens epithelium of early ARCC patients or transparent lens controls. Similarly, we observed no expression of the pyroptosis executor N-GSDMD, and levels of the ferroptosis marker GPX4 showed no significant differences between groups. Given the crucial role of autophagy in LEC homeostasis, we conducted a comprehensive analysis of key autophagy-related proteins. P62, a multifunctional protein, plays pivotal roles in autophagy, proteolysis, and aggregate formation.[30] During ER stress, a known trigger for paraptosis, P62 upregulation facilitates the degradation of accumulated unfolded and misfolded proteins.[31] BECN1 serves as a key initiator of autophagy, participating in autophagosome formation through complex protein interactions and promoting autophagic membrane development.[32] During the autophagic process, LC3-I is converted to LC3-II and associates with the autophagosome membrane, marking its maturation.[33] Our findings revealed elevated levels of both P62 and BECN1 in LECs from early ARCC patients, while LC3B expression remained unchanged. This suggests activation of the autophagy pathway, although autophagosome formation has not yet reached a level sufficient for effective substrate degradation. Our previous research demonstrated elevated levels of both LC3B and P62 in mature cataract patients, suggesting enhanced autophagic activity during ARC progression despite potential impairment in autophagic flux.[34] Hence, we concluded that paraptosis likely represents the predominant mode of cell death in LECs during early ARCC development.

ROS have been identified as primary initiators of paraptosis[26,35,36] and crucial risk factors in ARC pathogenesis.[37,38] DNA molecules exhibit particular vulnerability to ROS-mediated attacks, leading to oxidative damage and subsequent progression of age-related diseases.[21] We found elevated ROS levels in the lens epithelium of early ARCC. Our previous research indicated that the aberrant expression of oxidative damage repair proteins, such as Ku70 and OGG1, contributed to ARC development.[19,39] Notably, Ku70 depletion significantly elevated intracellular ROS levels, triggering cytoplasmic vacuolization and paraptosis.[40] This finding implies that dysfunction in oxidative damage repair proteins may initiate paraptosis through ROS-dependent mechanisms. Intriguingly, studies have indicated that diminished OGG1 function may induce cellular vacuolization in neuronal cells, although the precise molecular mechanisms remain to be elucidated.[41] OGG1, a specialized DNA repair enzyme, plays a pivotal role in the base excision repair pathway by specifically targeting and removing 8-oxoG, a critical marker of oxidative DNA damage.[42] Our previous research found that OGG1 protein expression was increased in the lens epithelium of ARC.[19] After paraptosis was induced in LECs by low concentrations of H_2O_2, the protein expression of OGG1 increased, yet the level of intracellular 8-oxoG remained significantly high. Further overexpression of OGG1 did not suppress paraptosis. Some researchers believe that elevated ROS levels during oxidative stress may inhibit the enzyme activity of OGG1 through posttranslational modifications.[43,44] The enzyme activity and functions of OGG1 may be impaired under oxidative damage. Therefore, merely increasing its protein content does not address the issue of inadequate repair functionality.

TH10785, a novel small-molecule synthetic compound, interacts with the phenylalanine-319 and glycine-42 amino acids of OGG1, enhancing enzyme activity by 10-fold.[45] In the present study, TH10785 augmented OGG1 recruitment to sites of DNA damage under oxidative stress conditions, thereby facilitating the repair of oxidative DNA lesions. Besides, TH10785 demonstrated significant efficacy in suppressing H_2O_2-induced LECs paraptosis. Conversely, inhibition of OGG1 activity by TH5487 resulted in exacerbation of paraptotic cell death. The therapeutic potential of TH10785 was further validated in an ex vivo rat model, where it effectively mitigated H_2O_2-induced paraptosis in LECs and significantly reduced the formation of cortical vacuoles in the lens. Therefore, our findings highlight the critical role of OGG1-mediated oxidative damage repair in preventing paraptosis in LECs. The specific activation of OGG1 by TH10785, characterized by minimal off-target effects, represents a promising therapeutic strategy for early intervention in ARCC. However, limited safety data

Investigative Ophthalmology & Visual Science

on the potential risks and contraindications associated with OGG1-targeted therapies are available from current studies. Further investigations utilizing rodent models are essential to comprehensively evaluate the pharmacokinetic properties, safety profile, and therapeutic efficacy of TH10785. We also propose to establish patient-specific ARCC models in vitro using mature lentoid bodies derived from human induced pluripotent stem cells.[46] This innovative approach will enable more precise and clinically relevant evaluation of TH10785's potential effects on human lens tissue, bridging the gap between preclinical research and clinical application. To enhance therapeutic outcomes while minimizing adverse effects, we will explore advanced drug delivery strategies by combining small molecules with either cell-penetrating peptides or engineered nanoparticles.[47] Such targeted delivery systems hold promise for improving ocular bioavailability and tissue-specific drug distribution. Through this comprehensive series of investigations, encompassing both fundamental research and translational studies, we aim to establish TH10785 as a novel, effective, and safe therapeutic strategy for early-stage ARCC intervention.

Taken together, our study reveals that ROS-induced paraptosis occurred in the LECs of patients with early ARCC. OGG1 plays a protective role in the paraptosis of LECs. TH10785 exhibits a potent capacity to activate OGG1 enzyme activity, effectively suppressing paraptosis in LECs and alleviating vacuolar degeneration in the superficial lens cortex (Fig. 5). These findings hold significant clinical potential, offering promising strategies for drug treatment in early ARCC.

Acknowledgments

Supported by research grants from the National Natural Science Foundation of China (82171038, 82101101), Jiangsu Provincial Research Hospital (YJXYY202204), Jiangsu Provincial Medical Key Discipline (JSDW202245), Jiangsu Commission of Health (M2021084), Postgraduate Research & Practice Innovation Program of Jiangsu Province (KYCX23_3430), the Science and Technology Project of Nantong Municipality (MS22022020), and Municipal Health Commission of Nantong (NTCXTD41).

Disclosure: **W. Geng**, None; **P. Li**, None; **G. Zhang**, None; **R. Zhong**, None; **L. Xu**, None; **L. Kang**, None; **X. Liu**, None; **M. Wu**, None; **M. Ji**, None; **H. Guan**, None

References

1. Hashemi H, Pakzad R, Yekta A, et al. Global and regional prevalence of age-related cataract: a comprehensive systematic review and meta-analysis. *Eye (Lond)*. 2020;34:1357–1370.
2. Chan E, Mahroo OA, Spalton DJ. Complications of cataract surgery. *Clin Exp Optom*. 2010;93:379–389.
3. Abdelkader H, Alany RG, Pierscionek B. Age-related cataract and drug therapy: opportunities and challenges for topical antioxidant delivery to the lens. *J Pharm Pharmacol*. 2015;67:537–550.
4. Jacob TJ. The relationship between cataract, cell swelling and volume regulation. *Prog Retin Eye Res*. 1999;18:223–233.
5. Tripathi RC, Tripathi BJ. Lens morphology, aging, and cataract. *J Gerontol*. 1983;38:258–270.
6. Wishart TFL, Flokis M, Shu DY, Das SJ, Lovicu FJ. Hallmarks of lens aging and cataractogenesis. *Exp Eye Res*. 2021;210:108709.
7. Hong Y, Sun Y, Ye X, et al. Prevalence and risk factors for adult cataract in the Jingan district of Shanghai. *J Ophthalmol*. 2022;2022:7547043.
8. Braakhuis AJ, Donaldson CI, Lim JC, Donaldson PJ. Nutritional strategies to prevent lens cataract: current status and future strategies. *Nutrients*. 2019;11:1186.
9. Yang T, Lin X, Li H, et al. Acetyl-11-keto-beta boswellic acid (AKBA) protects lens epithelial cells against H_2O_2-induced oxidative injury and attenuates cataract progression by activating Keap1/Nrf2/HO-1 signaling. *Front Pharmacol*. 2022;13:927871.
10. Xu Y, Zheng Y, Shen P, Zhou L. Role of long noncoding RNA KCNQ1 overlapping transcript 1/microRNA-124-3p/BCL-2-like 11 axis in hydrogen peroxide (H_2O_2)-stimulated human lens epithelial cells. *Bioengineered*. 2022;13:5035–5045.
11. Ma DY, Liu JX, Wang LD, et al. GSK-3β-dependent Nrf2 antioxidant response modulates ferroptosis of lens epithelial cells in age-related cataract. *Free Radic Biol Med*. 2023;204:161–176.
12. Huang J, Yu W, He Q, et al. Autophagy facilitates age-related cell apoptosis-a new insight from senile cataract. *Cell Death Dis*. 2022;13:37.
13. Vrensen G, Willekens B. Biomicroscopy and scanning electron microscopy of early opacities in the aging human lens. *Invest Ophthalmol Vis Sci*. 1990;31:1582–1591.
14. Jia DP, Wang S, Zhang BC, Fang F. Paraptosis triggers mitochondrial pathway-mediated apoptosis in Alzheimer's disease. *Exp Ther Med*. 2021;22:1280.
15. Wang Y, Wen X, Zhang N, et al. Small-molecule compounds target paraptosis to improve cancer therapy. *Biomed Pharmacother*. 2019;118:109203.
16. Wu J, Zhou J, Ping X, et al. Scanning and transmission electron microscopy study of anterior lens epithelium in presenile cataract. *Int Ophthalmol*. 2020;40:1411–1418.
17. Andjelic S, Drašlar K, Hvala A, Hawlina M. Structural characteristics of the lens in presenile cataract. *Front Med (Lausanne)*. 2021;8:802275.
18. Erol Tinaztepe Ö, Ay M, Eser E. Nuclear and mitochondrial DNA of age-related cataract patients are susceptible to oxidative damage. *Curr Eye Res*. 2017;42:583–588.
19. Kang L, Zhao W, Zhang G, Wu J, Guan H. Acetylated 8-oxoguanine DNA glycosylase 1 and its relationship with p300 and SIRT1 in lens epithelium cells from age-related cataract. *Exp Eye Res*. 2015;135:102–108.
20. Capes-Davis A, Reid YA, Kline MC, et al. Match criteria for human cell line authentication: where do we draw the line? *Int J Cancer*. 2013;132:2510–2519.
21. Zhong Y, Zhang X, Feng R, et al. OGG1: an emerging multifunctional therapeutic target for the treatment of diseases caused by oxidative DNA damage. *Med Res Rev*. 2024;44:2825–2848.
22. Hanna BMF, Helleday T, Mortusewicz O. OGG1 inhibitor TH5487 alters OGG1 chromatin dynamics and prevents incisions. *Biomolecules*. 2020;10:1483.
23. Sperandio S, Poksay K, de Belle I, et al. Paraptosis: mediation by MAP kinases and inhibition by AIP-1/Alix. *Cell Death Differ*. 2004;11:1066–1075.
24. Handayaningsih AE, Iguchi G, Fukuoka H, et al. Reactive oxygen species play an essential role in IGF-I signaling and IGF-I-induced myocyte hypertrophy in C2C12 myocytes. *Endocrinology*. 2011;152:912–921.
25. Sperandio S, de Belle I, Bredesen DE. An alternative, nonapoptotic form of programmed cell death. *Proc Natl Acad Sci USA*. 2000;97:14376–14381.
26. Chen X, Chen X, Zhang X, et al. Curcuminoid B63 induces ROS-mediated paraptosis-like cell death by targeting TrxR1 in gastric cells. *Redox Biol*. 2019;21:101061.

27. Hu S, Su D, Sun L, et al. High-expression of ROCK1 modulates the apoptosis of lens epithelial cells in age-related cataracts by targeting p53 gene. *Mol Med*. 2020;26:124.
28. Xiang J, Kang L, Gao H, et al. BLM can regulate cataract progression by influencing cell vitality and apoptosis. *Exp Eye Res*. 2019;178:99–107.
29. Wei Z, Hao C, Huangfu J, Srinivasagan R, Zhang X, Fan X. Aging lens epithelium is susceptible to ferroptosis. *Free Radic Biol Med*. 2021;167:94–108.
30. Zhou L, Wang H, Ren H, Hu Q, Ying Z, Wang G. Bcl-2 decreases the affinity of SQSTM1/p62 to poly-ubiquitin chains and suppresses the aggregation of misfolded protein in neurodegenerative disease. *Mol Neurobiol*. 2015;52:1180–1189.
31. Zaffagnini G, Savova A, Danieli A, et al. p62 filaments capture and present ubiquitinated cargos for autophagy. *EMBO J*. 2018;37:e98308.
32. Prerna K, Dubey VK. Beclin1-mediated interplay between autophagy and apoptosis: new understanding. *Int J Biol Macromol*. 2022;204:258–273.
33. Tanida I, Ueno T, Kominami E. LC3 and autophagy. *Methods Mol Biol*. 2008;445:77–88.
34. Cao Y, Li P, Zhang G, et al. MicroRNA Let-7c-5p-mediated regulation of ERCC6 disrupts autophagic flux in age-related cataract via the binding to VCP. *Curr Eye Res*. 2021;46:1353–1362.
35. Ghosh K, De S, Das S, Mukherjee S, Sengupta Bandyopadhyay S. Withaferin A induces ROS-mediated paraptosis in human breast cancer cell-lines MCF-7 and MDA-MB-231. *PLoS One*. 2016;11:e0168488.
36. Nguyen PL, Lee CH, Lee H, Cho J. Induction of paraptotic cell death in breast cancer cells by a novel pyrazolo[3,4-h]quinoline derivative through ROS production and endoplasmic reticulum stress. *Antioxidants (Basel, Switzerland)*. 2022;11:117.
37. Zhao C, Zeng H, Wu RT, Cheng WH. Loss of selenium-binding protein 1 decreases sensitivity to clastogens and intracellular selenium content in HeLa cells. *PLoS One*. 2016;11:e0158650.
38. Chen X, Li P, Zhang G, et al. Comprehensive profiling of proteome and ubiquitome changes in human lens epithelial cell line after ultraviolet-B irradiation. *ACS Omega*. 2020;5:32171–32182.
39. Zhang W, Wu A, Zhang G, et al. Ubiquitination of Ku70 by Parkin promotes apoptosis of lens epithelial cells. *FEBS J*. 2023;290:3828–3842.
40. Ding L, Wen Y, Zhang X, et al. Transcriptional network constituted of CBP, Ku70, NOX2, and BAX prevents the cell death of necrosis, paraptosis, and apoptosis in human melanoma. *Cell Death Discov*. 2021;7:40.
41. Murakami T, Nagai M, Miyazaki K, et al. Early decrease of mitochondrial DNA repair enzymes in spinal motor neurons of presymptomatic transgenic mice carrying a mutant SOD1 gene. *Brain Res*. 2007;1150:182–189.
42. Zhao F, Zhu J, Zhang M, et al. OGG1 aggravates renal ischemia-reperfusion injury by repressing PINK1-mediated mitophagy. *Cell Prolif*. 2023;56:e13418.
43. Vlahopoulos S, Adamaki M, Khoury N, Zoumpourlis V, Boldogh I. Roles of DNA repair enzyme OGG1 in innate immunity and its significance for lung cancer. *Pharmacol Ther*. 2019;194:59–72.
44. Bravard A, Vacher M, Gouget B, et al. Redox regulation of human OGG1 activity in response to cellular oxidative stress. *Mol Cell Biol*. 2006;26:7430–7436.
45. Michel M, Benítez-Buelga C, Calvo PA, et al. Small-molecule activation of OGG1 increases oxidative DNA damage repair by gaining a new function. *Science*. 2022;376:1471–1476.
46. Lyu D, Zhang L, Qin Z, et al. Modeling congenital cataract in vitro using patient-specific induced pluripotent stem cells. *NPJ Regen Med*. 2021;6:60.
47. Chen Y, Ye Z, Chen H, Li Z. Breaking barriers: nanomedicine-based drug delivery for cataract treatment. *Int J Nanomed*. 2024;19:4021–4040.

Investigative Ophthalmology & Visual Science